

BTSeg: Barlow Twins Regularization for Domain Adaptation in Semantic Segmentation

Johannes Künzel

Fraunhofer Institute for Telecommunications
Heinrich-Hertz-Institut, HHI

johannes.kuenzel@hhi.fraunhofer.de

Anna Hilsmann

Fraunhofer Institute for Telecommunications,
Heinrich-Hertz-Institut, HHI

anna.hilsmann@hhi.fraunhofer.de

Peter Eisert

Humboldt University Berlin

peter.eisert@hu-berlin.de

Abstract

Semantic image segmentation is a critical component in many computer vision systems, such as autonomous driving. In such applications, adverse conditions (heavy rain, night time, snow, extreme lighting) on the one hand pose specific challenges, yet are typically underrepresented in the available datasets. Generating more training data is cumbersome and expensive, and the process itself is error-prone due to the inherent aleatoric uncertainty. To address this challenging problem, we propose BTSeg, which exploits image-level correspondences as weak supervision signal to learn a segmentation model that is agnostic to adverse conditions. To this end, our approach uses the Barlow twins loss from the field of unsupervised learning and treats images taken at the same location but under different adverse conditions as "augmentations" of the same unknown underlying base image. This allows the training of a segmentation model that is robust to appearance changes introduced by different adverse conditions. We evaluate our approach on ACDC and the new challenging ACG benchmark to demonstrate its robustness and generalization capabilities. Our approach performs favorably when compared to the current state-of-the-art methods, while also being simpler to implement and train. The code will be released upon acceptance.

1. Introduction

Semantic segmentation of images is a longstanding and challenging task in the field of computer vision. This challenge becomes even more pronounced in domains such as autonomous driving, where adverse conditions like snow, heavy rain, fog, and night pose significant difficulties. The creation of highly accurate pixel-wise annotated train-

ing data is expensive and challenging, due to the inherent aleatoric uncertainty (where to draw the line between road and sidewalk in the presence of snow), which makes it necessary to use sophisticated annotations schemes like in [26]. As a result, modern data-driven methods work unreliably when confronted with such circumstances. Addressing this scarcity of training data, unsupervised domain adaption (UDA) methods [2–5, 17, 19] have been proposed. Recent datasets ([22, 26]) for semantic segmentation under adverse weather conditions pair the labeled adverse-condition images with a reference images, taken under clear conditions roughly matched based on GPS coordinates.

Taking advantage of these data, we introduce BTSeg (Barlow Twins regularized Segmentation), a new weather condition agnostic image segmentation model, which integrates the Barlow Twins approach [32], a self-supervised learning method based on redundancy-reduction into the classical learning of semantic segmentation. The original Barlow Twins approach involves creating two distinct augmentations (spatial distortions) of a single input image and training an encoder to be invariant to these augmentations (see Sec. 3.1 for a brief introduction). Inspired by this, we treat images captured under clear and adverse weather conditions at the same location as different augmentations of the same common underlying base image. By enforcing similarity of feature encodings through the Barlow Twins loss, we train the semantic segmentation network's backbone to extract the knowledge hidden in both images (see Fig. 1 for a conceptual diagram). Thereby, we can capitalize on the ground truth data obtained from clear weather instances, while using the annotated adverse weather images solely during evaluation. Leveraging the Barlow Twins approach results in several benefits: (i) it eliminates the need for negative sampling (unlike methods, such as [4]); (ii) it avoids the necessity of annotating the adverse weather

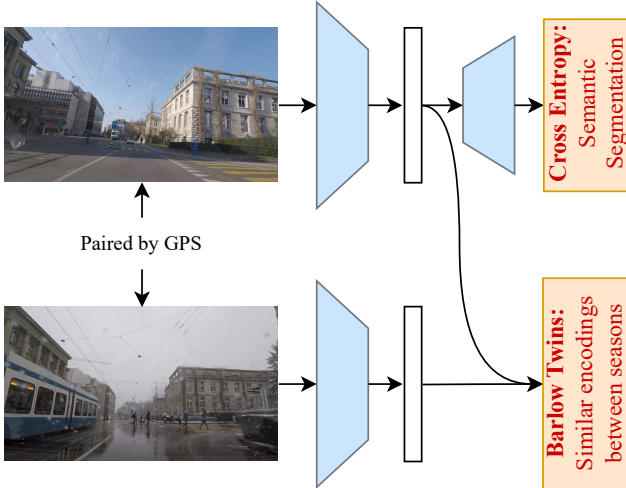


Figure 1. BTSeg integrates the Barlow Twins loss as regularization into a semantic segmentation network. The method takes two images as input, which are acquired at a similar location, but under differing weather conditions. From the Barlow Twins perspective, we treat them as two versions generated from an underlying base image through augmentation, namely, the varying weather conditions. The loss of the Barlow Twins prompts the segmentation backbone to produce encodings that (I) allow for accurate estimation of semantic segmentation and (II) are resilient to changes in appearance resulting from varying weather conditions.

images, and (iii) it is relatively simple to implement. Our approach can be easily be integrated into common semantic segmentation networks, which consist of a backbone and segmentation head part, and introduces only a negligibly increase in the number of parameters.

In the remainder of this paper, we review related publications in Sec. 2 and give a brief introduction to Barlow Twins (Sec. 3.1), before we explain our approach to integrate it with a semantic segmentation network (Sec. 3.2). We then show how to address insufficiently aligned image content in the training data (Sec. 3.3-Sec. 3.5) inherent to image pairs matched by their GPS positions only. In Sec. 4, we present a thorough evaluation of our approach: We evaluate our method against the strong state of the art, investigate the usefulness of our design choices and finally analyze the generalization and robustness. We conclude our paper with Sec. 5, providing a summary while highlighting the limitations and potential avenues for future research.

2. Related work

In this section, we briefly review the state-of-the-art in image segmentation under adverse conditions, self-supervised learning and combination thereof.

2.1. Weakly-supervised domain adaption

With the appearance of datasets like Dark Zurich [22] and ACDC [26], the landscape of datasets for semantic image segmentation experienced an important extension in the direction of adverse weather conditions. These datasets contain images captured with different lighting situations (nighttime, twilight, and daytime) or different adverse conditions (fog, nighttime, rain, snow). Each adverse-condition image contains a manually created semantic segmentation and is paired with a reference image taken under favorable weather conditions at almost the same viewpoint / location.

This prepared the ground for weakly-supervised domain adaption methods, which leverage the information hidden within this association.

Sakaridis et al. use daytime, twilight, and nighttime images to gradually adapt from the daytime to the nighttime domain [23]. To this end, their method extracts information from the reference-to-target-image pairing and the usage of artificially stylized annotated images. The usage of stylized images and the gradual adaption procedure were omitted by Bruggemann et al. [5]. Instead, an uncertainty-aware *ALIGN*-module was introduced to improve the alignment between reference and target domain.

In [4], Bruggemaqnn et al. use a contrastive loss formulation in the embedding space to learn features robust to the weather conditions. This procedure requires the maintenance of a list of negative samples for each positive sample, which complicates the implementation and can impede the training process, if the negative samples are too close to the positives.

2.2. Self-supervised learning

Self-supervised learning methods aim to extract valuable features from unlabeled input data. Instead of ground truth labels, these methods operate by applying synthetic augmentations to the input images to teach the network to create features robust against these augmentations. However, this naive approach can potentially lead to a degraded solution, where the network predicts a constant, data-independent feature representation. To avoid this trivial solution, a variety of methods has been proposed.

Contrastive-based methods like [8, 20] try to ensure that the embeddings of correlated images (referred to as positive samples) exhibit greater proximity compared to embeddings of unrelated images (considered as negative samples). Essential to these methods is the availability of appropriate negative examples to prevent the learning process stepping into a degenerated solution.

Clustering-based algorithms (such as proposed in [1, 6]) learn to assign an image with a corresponding cluster, while disregarding any augmentations that have been applied. However, careful control of the clustering is necessary to

prevent the trivial solution of assigning all embeddings to the same cluster.

The Barlow Twins methods proposed by Zbontar et al. [32] relies on redundancy reduction and avoids the usage of negative samples, asymmetric parameter updates, stopped gradient or non-differential operators. The trivial solution is solely avoided through the formulation of the loss, which enforces the cross-correlation between the batch-normalized embeddings of two distorted versions of a sample to resemble the identity matrix.

2.3. Barlow Twins for semantic segmentation

The Barlow Twins approach has been successfully applied for the segmentation of medical images [27], [21] and [21]. These methods use classical augmentation techniques to create two distorted versions from the same image, as in the original work [32].

The work of Bhagwatkar et al. in [3] exploits the Barlow Twins loss formulation [32] to train an encoder network robust against “domain transformations” and assumes “corresponding images from different domains as different views of the same abstract representation”. Additionally, they jointly train a segmentation head for one domain, utilizing the output of the backbone. However, they try to adapt from synthetic to real data, but remain unclear how to select corresponding images in this setting. Therefore, these images *do not share* semantically close content. In our opinion, this is detrimental for the training of the encoder, as it is consequently forced to generate similar embeddings for images with different content. Of course, this should result in an increased robustness against the “domain transformations”, but forces the backbone also to embed two different image contents, resulting in two contrary objectives.

In contrast to that, we use paired images of the same location, one acquired under clear and one under adverse conditions. Additionally, we take further steps to handle mobile content and misaligned viewpoints.

3. Method

This section describes our approach, leveraging the Barlow Twins loss to train semantic segmentation networks robust to domain changes. We start with a brief introduction of the original Barlow Twins objective in Sec. 3.1 and then describe our extension and integration into a semantic segmentation network in Sec. 3.2. In Sec. 3.3, Sec. 3.4 and Sec. 3.5 we describe how we account for semantically misaligned target and reference images.

3.1. Brief introduction to Barlow Twins

The Barlow Twins loss was introduced by Zbontar et al. in [32] and originates from the domain of self-supervised learning. In their approach, images from the training

dataset (\mathbf{X}) are passed through two randomized augmentation pipelines, each applying different augmentation techniques. This process creates two different versions (\mathbf{Y}_A and \mathbf{Y}_B) of the same original input image. Both images are passed through the same encoder (originally, a ResNet-50 without the final classification layer) which produces two *representations* of the input images. Afterwards, an average pooling layer squashes the representations maps to vectors which are further processed by an attached projection network (fully connected layers with ReLU activations and batch normalization in between). This results in *embedding* vectors, \mathbf{Z}_A and $\mathbf{Z}_B \in M_{b \times p}(\mathbb{R})$ with b being the number of batches and p the dimension of the embedding vector. The key idea of [32] is to normalize each dimension of the embedding vectors across its batch dimension and to use the resulting normalized vectors to calculate the cross-correlation matrix $\mathbf{C} \in M_{n \times n}(\mathbb{R})$. The proposed loss function

$$\mathcal{L}_{BT} = \sum_i (1 - \mathbf{C}_{ii})^2 + \lambda \sum_i \sum_{j \neq i} \mathbf{C}_{ij}^2 \quad (1)$$

enforces values of one on the diagonal of the matrix and zeros everywhere else (resembling the identity matrix), with $\lambda \in \mathbb{R}$ equilibrating both parts. In the loss function, the first part enforces invariance against the different augmentations applied and the second part reduces the information redundancy between the different dimensions of the feature vector. After utilizing Eq. (1) for pre-training, the encoder part can be fine-tuned for downstream tasks like the classification of images.

The main advantage arises from the absence of a requirement for negative samples, like for instance in contrastive losses. This simplifies the implementation and circumvents the need for choosing negative samples, a task prone to errors. Automatically selected negative samples often end up being too similar to the anchor, as discussed in Sec. 2.2.

3.2. Robust semantic segmentation through Barlow Twins

Fig. 2 depicts our network structure BTSeg for the integration of the Barlow Twins objective into semantic segmentation. The key idea is to use two images from the same location but different domains (*e.g.* different season, or weather conditions), and treat the appearance differences as augmentations of the same sample. In this section, we assume that both images were taken at the same location with the same viewpoint, therefore showing semantically aligned content (see Secs. 3.3 to 3.5).

Using the notation from domain adaptation, we denote the reference image taken under clear conditions as source image \mathbf{X}_s and the image taken under adverse conditions as target image \mathbf{X}_t . Both images \mathbf{X}_s and \mathbf{X}_t are passed through the backbone network f_θ resulting in the image features \mathbf{Y}_s and \mathbf{Y}_t . This process reduces the spatial dimen-

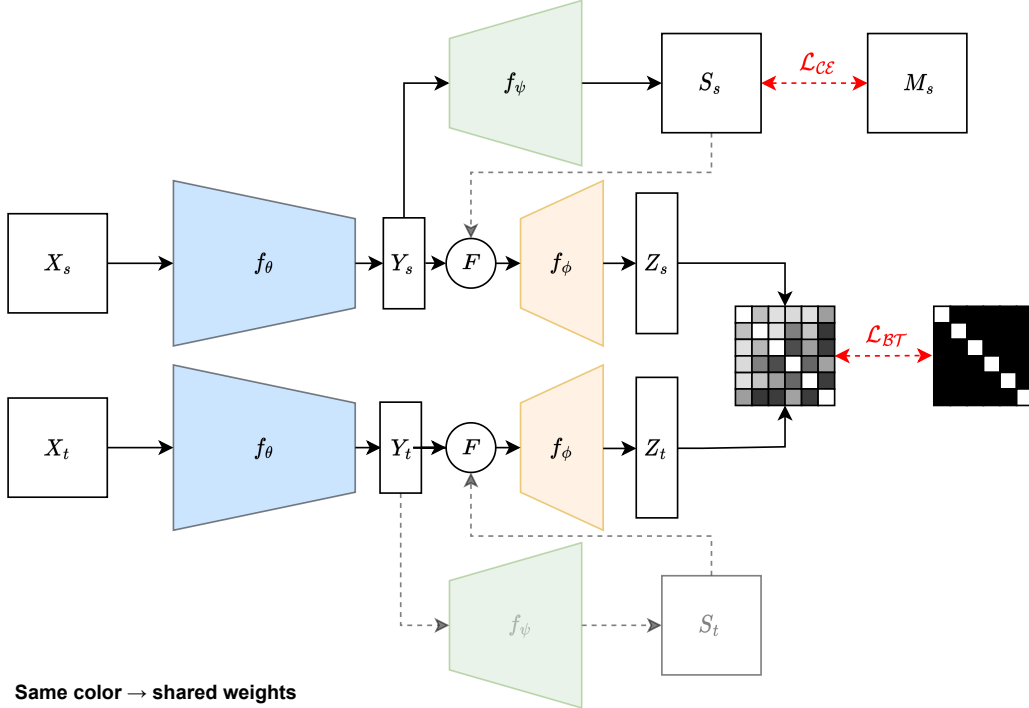


Figure 2. Schematic overview of our proposed semi-supervised semantic segmentation architecture, where the Barlow Twins loss enforces close embeddings for images (X_s and X_t) taken at the same location with differing environmental conditions.

sions from $b \times c \times h \times w$ to $b \times c \times m \times n$, with b being the number of batches, c the number of channels and the others specifying height and width, with $m, n < h, w$. A pooling layer F (usually an average pooling) further squashes the dimension to $b \times c \times 1 \times 1$, generating essentially a vector (y_s and y_t respectively) for each sample. Similar to the original Barlow Twins approach (described in Sec. 3.1), a fully-connected projection network f_ϕ generates the final embeddings $\mathbf{Z}_s, \mathbf{Z}_t \in M_{b \times p}(\mathbb{R})$ with p being the embedding dimension. These vectors are then normalized and correlated, resulting in the cross-correlation matrix $\mathbf{C} \in M_{n \times n}(\mathbb{R})$. This creates the first objective \mathcal{L}_{BT} (Eq. (1)) for the proposed network structure, to generate representations robust against the appearance changes between the different domains. We assume that the images of the source domain are acquired under favorable conditions (as for the reference images), allowing the generation of pixel-wise segmentation labels, generated either by manual annotation, or by training and applying a separate segmentation network. We call this domain the reference domain. The representations from the backbone are further processed by a segmentation head to generate a semantic segmentation $\mathbf{S}_s, \in M_{b \times m \times n}(\mathbb{R})$ of the reference domain, see Figure 2. We upscale the semantic segmentation \mathbf{S}_s with bilinear interpolation to match the input dimension. In conjunction with the ground truth data and the cross-entropy loss, this

provides a second objective \mathcal{L}_{CE} for the network, as it is forced to learn the semantic segmentation task. By combining both objectives with

$$\mathcal{L} = \mathcal{L}_{CE} + \alpha \mathcal{L}_{BT} \quad (2)$$

for a joint training, we force the backbone to learn representations which are robust against appearance changes between the domains while still being well-suited for the task of semantic segmentation. This enables the extraction of hidden knowledge and the training in a weakly-supervised manner for domains, where ground truth data is not available.

Please note that we do not utilize the annotated adverse weather images during training. Instead, we solely depend on the paired reference images. We argue that this approach is more productive since reference images are easier to annotate for practical applications.

This procedure assumes that appearance changes are caused by the domain-shift only and are not due to moving objects or different viewpoints. However, for images acquired under different adverse conditions in realistic scenarios, this cannot be guaranteed. In the following sections, we describe how we address the spatial misalignment in the training datasets.

3.3. Filtering of mobile classes

In order to account for misalignments in the datasets, we filter out moving objects (mobile classes) in the pooling operation during the training. To this end, we extended the default average pooling F with guidance from the segmentations (information flow indicated by dashed arrows from \mathcal{S}_f and \mathcal{S}_T to \mathcal{F} in Fig. 2). We generate a binary mask $\mathbf{B} \in M_{b \times m \times n}(\mathbb{R})$ from \mathbf{S} with

$$B_{i,j} = \begin{cases} 0 & \text{if } i, j \text{ was labeled as a mobile class} \\ 1 & \text{otherwise} \end{cases}, \quad (3)$$

to filter areas containing mobile classes by

$$y = \frac{\sum(\mathbf{Y} \odot \mathbf{B})}{\sum(\mathbf{B}) + \epsilon}, \quad (4)$$

with ϵ being some small constant for numerical stability, $\sum(\cdot)$ the sum over all elements in a matrix and \odot indicating the element-wise product between two matrices.

3.4. Pre-alignment of source and target

To reduce the influence of misalignments between the semantic content in the image pairs caused by slightly different viewpoints, we pre-align the target (adverse condition) to the reference (normal condition) image, utilizing the *UAWarpC*-module from [5], pre-trained in a self-supervised manner on MegaDepth [16]. The method returns a warp map aligning the two images, with zero indicating invalid regions (see Fig. 4). The later is used to find the largest intrinsic rectangle (marked red in Fig. 4) containing the valid warped image region, utilizing the algorithm¹ introduced in [18]. Reference, target and the reference segmentation are cropped accordingly.

3.5. Confidence-weighted averaging

The *UAWarpC*-module also outputs a confidence estimation (as depicted in Fig. 4d) $\mathbf{P}_W \in [0, 1]_{h \times w}$ for each warped image region. It assigns high confidence in well-matched image regions (like facades, poles, trees) and low confidence for rather texture-less regions (for instance sky and road). A low confidence is also assigned to moving objects, which we exploit by resizing the predicted feature maps to the input image size before calculating the average weighted with the confidence values.

4. Experiments

In this section, we first describe the datasets (Sec. 4.1) we use for training and evaluation as well as implementation details (Sec. 4.2). We then compare our method

¹Implementation from <https://github.com/OpenStitching/lir>

against the state of the art for unsupervised domain adaptation (Sec. 4.3) and evaluate the influence of our design choices in Sec. 4.4, the robustness and generalization capabilities in Sec. 4.5 and the influence of the batch size in Sec. 4.6.

4.1. Datasets

A-Cityscapes Halder et al. presented an extension of the ubiquitous Cityscapes dataset [9] to transfer the original input images from favorable to rainy and foggy driving conditions [11]. Each condition can be simulated in different levels of severity. The authors kindly provide the already augmented 2995 training images with a halved resolution of 1024 by 512 pixels. The rain intensity has eight intensity levels from 1mm/hr up to 200mm/hr. For our experiments, we only use the training images with a split of 0.8, 0.1 and 0.1 for training, validation and testing. We chose the rain images with 100mm/hr because we found them to be the most realistic. Please refer to Fig. 3 for sample images from the dataset.



Figure 3. Sample images of the A-Cityscapes dataset with clear and rainy (artificial) weather conditions.

ACDC Sakaridis et al. [26] published the ACDC dataset for semantic segmentation in autonomous driving under adverse conditions. For each weather condition (night, rain, fog, snow) 400 training and 100 validation (106 for night) and 500 testing images are available. Each one is paired with another image depicting the same scene from roughly the same viewpoint (matched via GPS) under favorable weather conditions. The dataset does not provide ground truth segmentations for the clear weather conditions. To generate these, we use the kindly provided models (trained on Cityscapes) from [28] to automatically generate the semantic segmentations for the reference images. The ACDC dataset provides segmentation masks for the adverse conditions. We use them only for validation.

ACG benchmark Bruggemann et al. proposed benchmark dataset to evaluate the generalization capabilities of models after domain adaptation [4]. The dataset was created through careful selection of images from WildDash2 [33], Foggy Zurich [10, 24], Foggy Driving [25] and BDD100K [31] and contains 121 images with fog, 225 with rain, 276 with snow, and 300 taken during nighttime conditions. In contrast to the ACDC dataset, this dataset includes

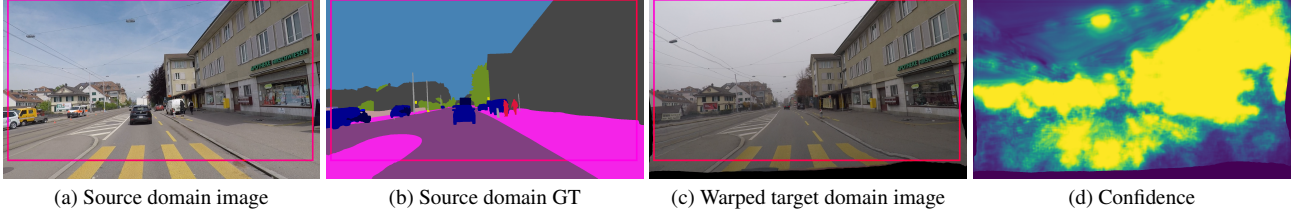


Figure 4. Sample image from the ACDC dataset with the image from the target domain warped to the source domain to align the semantics. The confidence map allows a prediction of the warp quality and is used as described in Sec. 3.5. The red rectangles denote the largest intrinsic rectangles containing only valid image content.

images with various combined adverse conditions, such as night-time rain, which makes it even more challenging.

4.2. Implementation details

Tsai et al. [29] proposed to set λ in Eq. (1) depending on the fraction of on-diagonal ($= n$) and off-diagonal ($= n(n-1)$) elements following

$$\frac{n}{n(n-1)} \approx \frac{1}{n} = \lambda. \quad (5)$$

We adopt this approach in order to avoid the necessity of tuning λ .

We pair our proposed Barlow Twins regularization with two semantic segmentation networks, *i.e.* DeeplabV3 [7] and SegFormer [30]. The integration of the DeeplabV3 architecture is straightforward, as it shares the ResNet-50 backbone with the original Barlow Twins implementation and outputs a 2048-dimensional feature map, which gets processed as described in Sec. 3.2. For the SegFormer architecture, we follow [4] and resize the outputs of the differently resolved transformer blocks to meet the resolution of the one with the highest resolution (one quarter of the input resolution) and concatenated the channels. This results in a 1024-dimensional feature map \mathbf{Y} , processed as described in Sec. 3.2.

For the fully-connected projection network, we use two layers only with a batch-normalization and a ReLU activation in between, squashing the input from 2048 (or 1024 for the SegFormer) to 512 and finally to 256. The original work from [32] projected the 2048-dimensional output of the encoder with three linear layers, each having 8192 units. During our experiments, we found no benefit in using such a huge fully-connected network.

During the training of our network, we took special care, to exclusively use complete batches. This is crucial as the Barlow Twins loss relies on a batch-normalization layer for its calculation. Failing to adhere to this practice results in spikes in the loss stemming from too small batches, insufficient for calculating the required statistics. To facilitate the learning process, we initialize the backbone of the DeeplabV3 architecture with weights obtained from pre-

training on ImageNet. Similarly, for the SegFormer architecture we initialize both the backbone and head with weights learned from Cityscapes dataset.

We train our model for 10000 steps on four GPUs with automatic mixed precision for the SegFormer architecture. In combination with a batch size of eight, this results in an effective batch size of 32 for the calculation of the Barlow Twins loss. During training, we use random cropping to 512 by 512 (768 by 768 when combined with DeeplabV3 and for SegFormer in our comparison to the state of the art in Sec. 4.3) and random horizontal flipping for data augmentation. We set $\alpha = 0.01$ in our combined objective function Eq. (2), to account for the different varying magnitudes of \mathcal{L}_{BT} and \mathcal{L}_{CE} . For the optimization, we use the AdamW optimizer with a weight decay of 0.01 in combination with a polynomial decay scheduler, for which we set the exponent to 0.9. Finally, we set the learning rates of the segmentation backbone and head to 0.0001 and of the projection network to 0.001, as it is the only randomly initialized part (following [4]).

4.3. Comparison to SOTA in semi-supervised domain adaptation

In Tab. 1, we compare our BTseg method against the state of the art for the domain adaptation from Cityscapes to ACDC. All methods have been evaluated on the official ACDC test set. The first line contains the baseline, a SegFormer [30] network trained solely on Cityscapes in a fully-supervised fashion. Due to the capable Transformer architecture, the baseline already shows good generalization properties outperforming MGCDA [23] and DAFormer [12] by a great margin. Our implementation, integrated into the DeeplabV3 [7] architecture, also falls behind this strong baseline, while also outperforming DAFormer and MGCDA. In combination with the SegFormer architecture, our method outperforms Refign [5] and CMA [4], while being less complex, as the Barlow Twins loss avoids the necessity of maintaining a list of negative samples, which are needed for the contrastive loss in CMA. Just as reported for CMA, our method also shows a good performance for mobile classes. This is remarkable, as these classes are es-

Table 1. Comparison to the state of the art in semi-supervised domain adaptation from Cityscapes \rightarrow ACDC, with the results reported on the official ACDC test set.

Architecture	Method	IoU \uparrow																			
		mean	road	sidewalk	building	wall	fence	pole	traffic light	traffic sign	vegetation	terrain	sky	person	rider	car	truck	bus	train	motorcycle	bicycle
SegFormer	Baseline	59.34	85.71	51.0	76.64	36.36	37.06	45.22	55.65	57.5	77.7	51.95	84.19	60.22	34.69	82.9	61.6	65.45	73.35	37.91	52.43
RefineNet	[23] MGCCA	48.65	73.1	29.01	70.01	19.2	26.44	36.68	52.66	53.24	75.04	31.7	84.75	50.61	25.67	77.7	43.14	45.78	54.98	32.9	41.67
DAFormer	[12] DAFormer	55.36	58.41	51.28	83.98	42.7	35.09	50.69	30.04	56.98	74.84	52.77	51.31	58.25	32.59	82.66	58.27	54.9	82.42	44.07	50.67
DAFormer	[5] Refign	65.51	89.48	63.44	87.3	43.62	34.33	52.28	63.21	61.38	86.94	58.45	95.66	62.14	39.3	84.07	65.7	71.33	85.42	47.94	52.79
SegFormer	[4] CMA	69.12	93.96	75.18	88.56	50.46	45.51	54.85	65.68	64.24	87.08	61.29	95.17	66.99	45.23	86.2	68.64	76.59	83.9	43.32	60.47
DAFormer	[5] Refign-HRDA	72.05	93.82	75.72	90.02	57.93	43.25	55.6	67.42	68.15	88.17	61.79	96.09	67.5	50.75	88.78	75.19	83.44	89.64	54.52	61.2
DeeplabV3	BTseg-DL (Ours)	56.12	89.78	63.98	82.99	33.34	37.61	50.56	62.45	58.42	81.9	48.94	93.92	53.7	17.46	80.	30.92	32.55	74.71	31.93	40.23
SegFormer	BTseg (Ours)	70.12	93.4	74.32	89.19	55.1	46.77	58.24	67.98	68.01	87.41	61.15	95.93	67.78	43.5	89.33	66.72	69.83	86.86	50.66	60.07

Table 2. Results of the ablation study performed on the ACDC validation subset reporting the IoU. "BT": usage of the Barlow Twins loss.

Methods				IoU \uparrow																			
BT	Warp	Crop	Pooling	mean	road	sidewalk	building	wall	fence	pole	traffic light	traffic sign	vegetation	terrain	sky	person	rider	car	truck	bus	train	motorcycle	bicycle
							Average	58.32	86.67	51.88	73.01	41.1	36.76	44.41	60.4	57.08	75.73	29.91	96.79	57.4	44.86	74.66	66.62
			Average	64.18	90.33	67.43	82.94	47.50	39.14	56.07	74.11	59.40	78.08	39.77	87.63	62.97	37.88	84.32	70.23	79.51	80.73	46.06	35.26
	x		Average	65.46	91.08	69.50	83.47	49.31	37.53	58.67	73.90	60.31	79.95	42.51	88.76	61.25	42.50	85.22	70.93	86.78	82.63	48.23	31.26
	x	x	Average	65.71	90.11	66.50	84.25	48.49	39.67	58.16	72.48	61.11	80.16	42.86	89.18	59.48	40.28	85.39	72.57	86.18	84.43	49.34	37.80
	x	x	Segmentation	65.42	89.74	67.31	83.85	48.88	38.07	59.33	73.19	60.74	80.23	42.83	88.51	59.65	40.34	85.13	75.41	86.07	81.32	48.84	33.50
	x	x	Confidence	65.23	89.74	66.01	84.02	49.62	39.34	58.70	74.01	61.39	79.78	43.65	88.62	60.66	42.58	84.69	73.46	85.46	72.26	49.43	35.91
	x	x	Conf. + Seg.	66.20	90.07	67.80	84.17	50.50	39.00	59.92	74.03	61.40	80.32	43.21	88.63	61.04	44.23	84.86	76.50	86.96	83.53	49.02	32.54

pecially challenging to our proposed method, as they violate our assumption of shared content between reference and target image. We suspect, that this was enabled through the rather coarse regularization, due to the squashing of the $c \times m \times n$ -dimensional feature map to a $c \times 1 \times 1$ -dimensional feature vector. The combination of Refign and HRDA [13] outperforms our method; however, it is considerably more complex and was trained on input images with a resolution of 1080 pixels, whereby we only train on 768 pixels, due to memory constraints. In summary, it can be stated that our method performs similarly to the state-of-the-art, despite being the only one not trained with full resolution. Considering this, it should be noted that training with images of 768 by 768 pixels instead of 512 by 512 already resulted in an approximate 2% increase in mIoU.

4.4. Ablation study

In this section, we analyze and evaluate our design choices. All numbers are from the ACDC validation set and we used the configuration described in Sec. 4.2 as foundation.

Tab. 2 shows the IoU values for the different classes present in the ACDC dataset and the overall mean, respectively. The first row shows the results if we train on the

labeled reference images only and evaluate on the target images. This results in a mean IoU of 58.32. The second row reports the results with our Barlow Twins regularization to enforce the segmentation backbones to be robust against the appearance changes caused by the different weather conditions. Subsequently, the mean IoU improves significantly by 5.86. Next, the warping/ alignment between reference and target image is added, improving the overall result to 65.5 (third row). The cropping of invalid image regions after the warping process brings another slight improvement. Interestingly, the result slightly decreases when we add segmentation or confidence guided averaging. For the later, this is probably caused by the overly pessimistic confidence estimations in homogeneous image regions, which may impede the training. The segmentation guided averaging is of course susceptible to misclassified image regions, and obstructs the learning of robust encoding, if mobile classes by chance align. Finally, the combination of both methods results in our best performing configuration with a mean IoU of 66.2.

In summary, the results show the intrinsic robustness of the proposed Barlow Twins regularization against slight misalignments, which could be interpreted as natural augmentations additional to the appearance changes caused by

Table 3. Comparison against the state of the art on the ACG benchmark (introduced in [4]), for the evaluation of robustness and generalization.

Method	mIoU \uparrow				
	fog	night	rain	snow	all
[12]DAFormer	52.6	21.5	47.5	33.6	40.1
[13]HRDA	60.0	27.1	56.2	43.3	48.9
[4]CMA	59.7	40.0	59.6	52.2	51.3
BTSeg (Ours)	60.7	35.7	56.1	49.1	48.1

the weather conditions.

4.5. Generalization and robustness

The authors of [4] proposed the new composed ACG benchmark to test the robustness and generalization capabilities of networks after the domain adaption from normal to adverse conditions. Tab. 3 shows the results from recent works, evaluated after the domain adaptation from Cityscapes to ACDC. Our method outperforms the state of the art for the fog subset. For the night subset, it improves significantly over DAFormer and HRDA, but falls behind CMA. Note that the night subset is especially challenging, as it also contains images from the other domains but at nighttime, which were not present in the ACDC dataset. For the rain subset, BTSeg is almost on par with HRDA and comparable to CMA. Again, for the snow subset it improves upon DAFormer and HRDA, but falls behind CMA.

We conclude, that our method shows robust performance in the presence of unseen data and even more challenging weather conditions.

4.6. Influence of the Batch Size

The original Barlow Twins paper [32] used a batch size of 2048, but reported also good results for batch sizes as small as 128. This smaller batch size of 128 was also used in [29], where much smaller datasets had been used (Tiny-Imagenet [15] and CIFAR-10 [14]). As our datasets are even smaller and the SegFormer architecture needs a lot of memory, we evaluated the performance of our proposed system for batch sizes from 8 to 32. We trained BTSeg with the configuration described in Sec. 4.2, but with only one to four graphic cards, resulting in an effective batch size for the Barlow Twins loss from 8 to 32. The resulting mean IoU values on the ACDC validation set are shown in Fig. 5. This makes it evident that an effective batch size below 24 impedes the statistics in the batch normalization layer of the Barlow Twins loss, therefore rendering the regularization unstable.

4.7. Robustness to misalignment

As Tab. 2 already indicated that our method is robust against misalignments between source (reference) and tar-

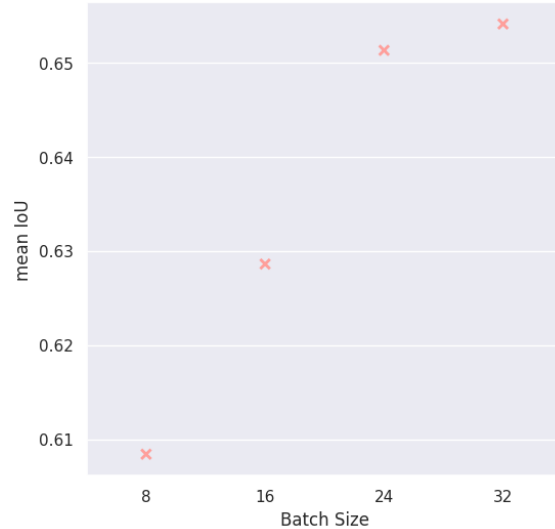


Figure 5. Influence of the batch size hyper parameter on the mean IoU, evaluated on the official ACDC validation set for all conditions.

get, we investigated this topic further. For this purpose, we trained BTSeg in combination with DeeplabV3 on the Cityscapes-A dataset. As training data we used the original Cityscapes images as reference and the images augmented with 100mm/h of rain as target. This simulates perfect conditions for our method, as the segmentation map of the source domain is identical to the target domain and the rain streaks act like a randomized augmentation, just like originally intended in [32]. Under these conditions, BT-Seg in conjunction with DeeplabV3 achieves a mean IoU of 66.12 on the Cityscapes validation set. We then introduced randomized affine transformations on the target images, simulating misaligned source and target images, like they can occur under real conditions due to inaccuracies in the GPS-based matching. Doing so results in a mean IoU of 63.08, which is only slightly worse compared to the previous result. This corroborates that BT-Seg is fairly robust against misalignments between target and reference. We hypothesize that this is made possible by the projection network and the averaging operation, which in combination lead to a focus on the general appearance change caused by the weather conditions, while still allowing the backbone to produce feature maps focusing on the image details.

5. Conclusion

In this paper, we presented BT-Seg, a domain adaptation method for semantically segmenting images captured in challenging weather conditions. To achieve this goal, we view images of a particular location captured under varying weather conditions as modifications of a shared, unknown

base image. By utilizing the Barlow Twins loss, we compel the segmentation backbone to withstand these assumed augmentations, *i.e.* different weather conditions. In contrast to the state of the art, this approach eliminates the need for selecting negative samples during training. Our approach performs well in comparison to the strong state of the art with the added benefits of being more straightforward to implement and train. In the future, we will examine strategies to lessen hardware demands caused by the implementation of batch normalization in the loss function. This necessitates the use of large batch sizes, which results in substantial memory requirements when paired with current models for semantic segmentation.

6. Acknowledgement

This work is supported by the the state of Berlin within the innovation support program ProFIT (IBB) (BerDiBa, grant no. 10185426) and by the German Federal Ministry for Economic Affairs and Climate Action (GEMIMEG-II, grant no. 01MT20001D).

References

- [1] Yuki M. Asano, Christian Rupprecht, and Andrea Vedaldi. Self-labelling via simultaneous clustering and representation learning. In *International Conference on Learning Representations (ICLR)*, 2020. 2
- [2] Sherwin Bahmani, Oliver Hahn, Eduard Zamfir, Nikita Araslanov, Daniel Cremers, and Stefan Roth. Semantic Self-adaptation: Enhancing Generalization with a Single Sample. *arXiv*, 2022. 1
- [3] Rishika Bhagwatkar, Saurabh Kemekar, Vinay Domatoti, Khurshed Munir Khan, and Anamika Singh. Contrastive Learning-Based Domain Adaptation for Semantic Segmentation. *2022 National Conference on Communications (NCC)*, 00:239–244, 2022. 1, 3
- [4] David Bruggemann, Christos Sakaridis, Tim Brödermann, and Luc Van Gool. Contrastive Model Adaptation for Cross-Condition Robustness in Semantic Segmentation. *arXiv*, 2023. 1, 2, 5, 6, 7, 8
- [5] David Bruggemann, Christos Sakaridis, Prune Truong, and Luc Van Gool. Refign: Align and Refine for Adaptation of Semantic Segmentation to Adverse Conditions. *2023 IEEE/CVF Winter Conference on Applications of Computer Vision (WACV)*, 00:3173–3183, 2023. 1, 2, 5, 6, 7
- [6] Mathilde Caron, Ishan Misra, Julien Mairal, Priya Goyal, Piotr Bojanowski, and Armand Joulin. Unsupervised learning of visual features by contrasting cluster assignments. In *Proceedings of Advances in Neural Information Processing Systems (NeurIPS)*, 2020. 2
- [7] Liang-Chieh Chen, George Papandreou, Florian Schroff, and Hartwig Adam. Rethinking Atrous Convolution for Semantic Image Segmentation. *arXiv*, 2017. 6
- [8] Ting Chen, Simon Kornblith, Mohammad Norouzi, and Geoffrey Hinton. A simple framework for contrastive learning of visual representations. In *International conference on machine learning*, pages 1597–1607. PMLR, 2020. 2
- [9] Marius Cordts, Mohamed Omran, Sebastian Ramos, Timo Rehfeld, Markus Enzweiler, Rodrigo Benenson, Uwe Franke, Stefan Roth, and Bernt Schiele. The Cityscapes Dataset for Semantic Urban Scene Understanding. In *IEEE Conference on Computer Vision and Pattern Recognition (CVPR)*, pages 3213–3223, 2016. 5
- [10] Dengxin Dai, Christos Sakaridis, Simon Hecker, and Luc Van Gool. Curriculum model adaptation with synthetic and real data for semantic foggy scene understanding. *International Journal of Computer Vision*, 128:1182–1204, 2019. 5
- [11] Shirsendu Sukanta Halder, Jean-François Lalonde, and Raoul de Charette. Physics-Based Rendering for Improving Robustness to Rain. *2019 IEEE/CVF International Conference on Computer Vision (ICCV)*, 00:10202–10211, 2019. 5
- [12] Lukas Hoyer, Dengxin Dai, and Luc Van Gool. DAFormer: Improving Network Architectures and Training Strategies for Domain-Adaptive Semantic Segmentation. *2022 IEEE/CVF Conference on Computer Vision and Pattern Recognition (CVPR)*, 00:9914–9925, 2022. 6, 7, 8
- [13] Lukas Hoyer, Dengxin Dai, and Luc Van Gool. HRDA: Context-Aware High-Resolution Domain-Adaptive Semantic Segmentation. In *European Conference on Computer Vision*, pages 372–391. Springer, 2022. 7, 8
- [14] Alex Krizhevsky. Learning multiple layers of features from tiny images. 2009. 8
- [15] Ya Le and Xuan S. Yang. Tiny imagenet visual recognition challenge. 2015. 8
- [16] Zhengqi Li and Noah Snavely. MegaDepth: Learning Single-View Depth Prediction from Internet Photos. *2018 IEEE/CVF Conference on Computer Vision and Pattern Recognition*, pages 2041–2050, 2018. 5
- [17] Fengmao Lv, Tao Liang, Xiang Chen, and Guosheng Lin. Cross-Domain Semantic Segmentation via Domain-Invariant Interactive Relation Transfer. *2020 IEEE/CVF Conference on Computer Vision and Pattern Recognition (CVPR)*, 00:4333–4342, 2020. 1
- [18] Zahraa Marzeh, Maryam Tahmasbi, and Narges Mirehi. Algorithm for finding the largest inscribed rectangle in polygon. *Journal of Algorithms and Computation*, 51(1):29–41, 2019. 5
- [19] M. Jehanzeb Mirza, Marc Masana, Horst Possegger, and Horst Bischof. An Efficient Domain-Incremental Learning Approach to Drive in All Weather Conditions. *2022 IEEE/CVF Conference on Computer Vision and Pattern Recognition Workshops (CVPRW)*, 00:3000–3010, 2022. 1
- [20] Ishan Misra and Laurens van der Maaten. Self-supervised learning of pretext-invariant representations. In *CVPR*, 2020. 2
- [21] Narinder Singh Punn and Sonali Agarwal. BT-Unet: A self-supervised learning framework for biomedical image segmentation using barlow twins with U-net models. *Machine Learning*, 111(12):4585–4600, 2022. 3
- [22] Christos Sakaridis, Dengxin Dai, and Luc Van Gool. Guided Curriculum Model Adaptation and Uncertainty-Aware Evaluation for Semantic Nighttime Image Segmentation. *2019*

- IEEE/CVF International Conference on Computer Vision (ICCV)*, 00:7373–7382, 2019. 1, 2
- [23] Christos Sakaridis, Dengxin Dai, and Luc Van Gool. Map-Guided Curriculum Domain Adaptation and Uncertainty-Aware Evaluation for Semantic Nighttime Image Segmentation. *IEEE Transactions on Pattern Analysis and Machine Intelligence*, 44(6):3139–3153, 2022. 2, 6, 7
- [24] Christos Sakaridis, Dengxin Dai, Simon Hecker, and Luc Van Gool. Model adaptation with synthetic and real data for semantic dense foggy scene understanding. In *European Conference on Computer Vision (ECCV)*, pages 707–724, 2018. 5
- [25] Christos Sakaridis, Dengxin Dai, and Luc Van Gool. Semantic foggy scene understanding with synthetic data. *International Journal of Computer Vision*, 126(9):973–992, Sep 2018. 5
- [26] Christos Sakaridis, Dengxin Dai, and Luc Van Gool. Acdc: The adverse conditions dataset with correspondences for semantic driving scene understanding. In *Proceedings of the IEEE/CVF International Conference on Computer Vision*, pages 10765–10775, 2021. 1, 2, 5
- [27] Md Mahfuzur Rahman Siddiquee and Andriy Myronenko. Brainlesion: Glioma, Multiple Sclerosis, Stroke and Traumatic Brain Injuries, 7th International Workshop, BrainLes 2021, Held in Conjunction with MICCAI 2021, Virtual Event, September 27, 2021, Revised Selected Papers, Part II. *Lecture Notes in Computer Science*, pages 163–172, 2022. 3
- [28] Andrew Tao, Karan Sapra, and Bryan Catanzaro. Hierarchical Multi-Scale Attention for Semantic Segmentation. *arXiv*, 2020. 5
- [29] Yao-Hung Hubert Tsai, Shaojie Bai, Louis-Philippe Morency, and Ruslan Salakhutdinov. A Note on Connecting Barlow Twins with Negative-Sample-Free Contrastive Learning. *arXiv*, 2021. 6, 8
- [30] Enze Xie, Wenhai Wang, Zhiding Yu, Anima Anandkumar, Jose M Alvarez, and Ping Luo. SegFormer: Simple and Efficient Design for Semantic Segmentation with Transformers. *Advances in Neural Information Processing Systems*, 34:12077–12090, 2021. 6
- [31] Fisher Yu, Haofeng Chen, Xin Wang, Wenqi Xian, Yingying Chen, Fangchen Liu, Vashisht Madhavan, and Trevor Darrell. Bdd100k: A diverse driving dataset for heterogeneous multitask learning. *2020 IEEE/CVF Conference on Computer Vision and Pattern Recognition (CVPR)*, pages 2633–2642, 2018. 5
- [32] Jure Zbontar, Li Jing, Ishan Misra, Yann LeCun, and Stéphane Deny. Barlow twins: Self-supervised learning via redundancy reduction. In *International Conference on Machine Learning*, pages 12310–12320. PMLR, 2021. 1, 3, 6, 8
- [33] Oliver Zendel, Matthias Schörghuber, Bernhard Rainer, Markus Murschitz, and Csaba Beleznai. Unifying panoptic segmentation for autonomous driving. In *Proceedings of the IEEE/CVF Conference on Computer Vision and Pattern Recognition (CVPR)*, pages 21351–21360, June 2022. 5